Vol 16 No 7, July 2007
1009-1963/2007/16(07)/2015-08

Chinese Physics

© 2007 Chin. Phys. Soc.
and IOP Publishing Ltd

Semi-vectorial analysis of a compact wavelength demultiplexer based on the tapered multimode interference coupler*

Xiao Jin-Biao(肖金标), Liu Xu(刘 旭),
Cai Chun(蔡 纯), and Sun Xiao-Han(孙小菡)

Lab of Photonics and Optical Communications, Electronic Engineering Department, Southeast University, Nanjing 210096, *China*

(Received 26 June 2006; revised manuscript received 11 January 2007)

Based on a parabolically tapered multimode interference (MMI) coupler with a deep-etched SiO_2/SiON rib waveguide, a compact wavelength demultiplexer operating at 1.30 and 1.55 μm wavelengths is proposed and analysed by using three-dimensional semi-vectorial finite-difference beam propagation method (3D-SV-FD-BPM). The results show that a MMI section of 330.0 μm in length, which is only 76% length of a straight MMI coupler, is achieved with the contrasts of 42.3 and 39.2dB in quasi-TE mode, and 38.4 and 37.8dB in quasi-TM mode at wavelengths 1.30 and 1.55 μm, respectively, and the insertion losses below 0.2dB at both wavelengths and in both polarization states. The alternating direction implicit algorithm with the Crank–Nicholson scheme is applied to the discretization of the 3D-SV-FD-BPM formulation along the longitudinal direction. Moreover, a modified FD scheme is constructed to approximate the resulting equations along the transverse directions, in which the discontinuities of the derivatives of magnetic field components H_y and H_x along the vertical and horizontal interfaces, respectively, are involved.

Keywords: wavelength demultiplexer, multimode interference, beam propagation method, photonic integrated circuits

PACC: 4280S, 4282, 4110H

1. Introduction

Wavelength division multiplexing (WDM) technology has been used to increase the number of channels and the information capacity in optical fibre communication.[1] The wavelength demultiplexers (or multiplexers) are essential components which separate (or combine) wavelengths carrying different information in WDM transmission system from (or with) each other.[1] Moreover, for optical telecommunications, much interest has been aroused in demultiplexing two wavelengths in 1.30 and 1.55 μm windows.[2]

Several devices have been proposed to perform this function, such as conventional directional couplers,[3] asymmetric Y-branch devices,[4] Mach–Zehnder interferometers,[5] and multimode interference (MMI) couplers.[6−8] Among them, the MMI-based devices have been attracted much attention due to their excellent characteristics, including easy fabrication, large optical bandwidth, low polarization dependence, and small size.[9,10] Soldano and Pennings showed the principles and applications of the MMI-based devices,[9] and Bachmann *et al* derived the self-imaging properties of generalized[11] and restricted[12] $N \times N$ MMI couplers. Several groups[7,8] have reported wavelength demultiplexers operating at 1.30 and 1.55 μm wavelengths based on MMI couplers. However, the length of these devices is still relatively large because the straight MMI couplers are used. Recently, Levy *et al* have demonstrated that the tapered MMI structures have a reduction in length compared with the straight MMI coupler.[13] The reduction in length is achieved in the tapered device by reducing the average MMI region width over the length of the structure. To the best of our knowledge, there has been no attempt so far to design a wavelength demultiplexer for the operation $\lambda = 1.30$ and 1.55 μm, based on the tapered MMI couplers. On the other hand, the three-dimensional (3D) finite difference (FD) beam propagation method (3D-FD-BPM), which automatically includes the effects of guided and radiating fields and mode coupling and conversion, has been widely

*Project supported by the Specialized Research Fund for the Doctoral Program of Higher Education of China (Grant No 20060286042).

used to design the MMI-based devices.[14] The scalar 3D-BPM holds only for the dielectric structures with a very small refractive index difference,[15] whilst the dielectric structures with a large refractive index difference in regions of high field intensity can be analysed by using the full-vectorial 3D-BPM,[16] but there is a great increase in computational time and cost. Instead, the semi-vectorial 3D-BPM is a good candidate for simulating the MMI-based devices, in which the polarization effects can be taken into account, but the memory requirement is the same as that in solving the scalar 3D-BPM. As a result, the computational time is moderate.[17]

In this paper, a wavelength demultiplexer operating at $\lambda = 1.30$ and $1.55\,\mu$m, based on the parabolically tapered MMI coupler, is analysed by using the three-dimensional semi-vectorial finite-difference beam propagation method (3D-SV-FD-BPM) based on H field. The present demultiplexer has the advantages of low loss, small polarization dependence, and compact size because the parabolically tapered MMI coupler based on the deep-etched SiO_2/SiON rib waveguide is used. The alternating direction implicit (ADI) algorithm with the Crank–Nicholson (CN) scheme is utilized to discretize the 3D-SV-FD-BPM formulation along the longitudinal direction (z-direction), which is numerically unconditionally stable and is of second-order accuracy in the z-direction. The calculation is efficient since the resulting matrix is tridiagonal. Moreover, a modified FD scheme based on the Taylor-series expansion is constructed to approximate the resulting equations along the transverse directions (x- and y-directions), in which the discontinuities of the derivatives of magnetic field components H_y and H_x along the vertical and horizontal interfaces, respectively, are involved. Compared with the local guided-modes analysis,[6,7,9], the 3D-SV-FD-BPM can not only reveal the optical wave propagation in the tapered MMI coupler, but can also evaluate the interaction between the output S-bent waveguides combined with the conformal mapping method.[18]

2. Computational method

The 3D-SV-FD-BPM based on H-field is employed to analyse the present wavelength demultiplexer. The basic equation for quasi-TE mode is expressed as[14]

$$\frac{\partial H_y}{\partial z} = (A_x + A_y)\, H_y \tag{1}$$

with

$$A_x H_y = \frac{1}{2\mathrm{j}k_0\bar{n}}\left[n^2\frac{\partial}{\partial x}\left(\frac{1}{n^2}\frac{\partial H_y}{\partial x}\right) + \frac{1}{2}k_0^2\left(n^2 - \bar{n}^2\right)H_y\right], \tag{2a}$$

$$A_y H_y = \frac{1}{2\mathrm{j}k_0\bar{n}}\left[\frac{\partial^2 H_y}{\partial y^2} + \frac{1}{2}k_0^2\left(n^2 - \bar{n}^2\right)H_y\right]. \tag{2b}$$

where k_0 is the wavenumber in free space, $\bar{n}$ is the reference refractive index, and $n(x, y, z)$ is the refractive index of the guiding medium. It is noted that A_x and A_y are the x- and y-dependent operators, respectively. For the quasi-TM mode analysis, the derivatives with respect to the x- and y-directions are interchanged. The ADI algorithm with the CN scheme, which is of second-order accuracy in the z-direction, is utilized to discretize Eq.(1) along the longitudinal direction. The discretization form becomes[19]

$$\left(1 - \frac{\Delta z}{2}A_x\right)\left(1 - \frac{\Delta z}{2}A_y\right)H_y^{l+1} = \left(1 + \frac{\Delta z}{2}A_x\right)\left(1 + \frac{\Delta z}{2}A_y\right)H_y^{l}. \tag{3}$$

Using the Peaceman–Rachford splitting technique,[19] one propagation step can be split into two sub-steps, which are summarized as follows:

1) First sub-step: $z = l\Delta z \to \left(l + \frac{1}{2}\right)\Delta z$,

$$\left(1 - \frac{\Delta z}{2}A_x\right)H_y^{l+\frac{1}{2}} = \left(1 + \frac{\Delta z}{2}A_y\right)H_y^{l}; \tag{4a}$$

2) Second sub-step: $z = \left(l + \frac{1}{2}\right)\Delta z \to (l+1)\Delta z$,

$$\left(1 - \frac{\Delta z}{2}A_y\right)H_y^{l+1} = \left(1 + \frac{\Delta z}{2}A_x\right)H_y^{l+\frac{1}{2}}. \tag{4b}$$

The resulting matrix at each sub-step is tridiag-

onal, thus the calculation is efficient. Moreover, it is shown by the von Neumann analysis that Eq.(3) is numerically unconditionally stable.[19]

Next, we construct the FD scheme to approximate the operators A_x and A_y along the transverse directions. The waveguide structure is scanned with the small rectangular sub-regions of size $\Delta x \times \Delta y$. Inside each sub-region the refractive index is constant, so the discontinuities of the refractive index profile occur only at the boundaries between adjacent sub-regions. The general situation for an arbitrary grid point (p, q, l) with neighbouring points is illustrated in Fig.1. The refractive indices for these points are denoted as $n_{p,q,l}$, $n_{p-1,\ q,l}$, $n_{p+1,\ q,\ l}$, $n_{p,q+1,\ l}$, and $n_{p,q-1,\ l}$, respectively.

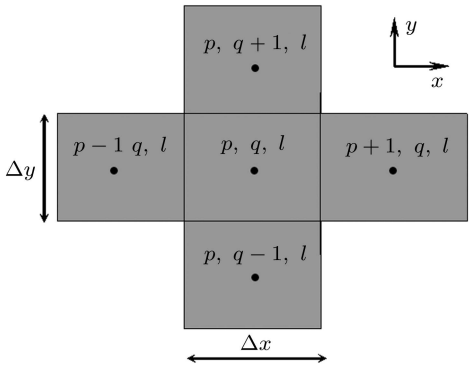


Fig.1. Point (p, q, l) and its neighbouring points.

Because H_y and its derivatives with respective to y are continuous across the horizontal interface, Eq.(2b) can be approximated with the conventional three-point difference, that is

$$A_y H_y \approx \frac{1}{2\mathrm{j}k_0\bar{n}}\left[\frac{H_y^{p,q+1,l}-2H_y^{p,q,l}+H_y^{p,q-1,l}}{(\Delta y)^2}+\frac{1}{2}k_0^2(n_{p,q,l}^2-\bar{n}^2)H_y^{p,q,l}\right]. \tag{5a}$$

When there exists an index discontinuity between (p,q,l) and (p+1,q,l) (or between ($p-1$, q, l) and (p, q, l)), H_y is still continuous, but its derivatives with respective to x are discontinuous. So the FD scheme must be modified to consider such discontinuities in Eq.(2a). By using the Taylor-series expansion, a modified FD scheme[20] is constructed, and given below:

$$A_y H_y \approx \frac{1}{2\mathrm{j}k_0\bar{n}}\left[\frac{\delta_1 H_y^{p-1,q,l}-\delta_2 2H_y^{p,q,l}+\delta_3 H_y^{p+1,q,l}}{\delta_4(\Delta y)^2}+\frac{1}{2}k_0^2(n_{p,q,l}^2-\bar{n}^2)H_y^{p,q,l}\right] \tag{5b}$$

with

$$\delta_1=\frac{n_{p,q,l}^2+n_{p+1,q,l}^2}{2n_{p,q,l}^2}+\sigma\left(\Delta x\right)^2\tau, \tag{6a}$$

$$\delta_2=\frac{3n_{p,q,l}^2+n_{p+1,q,l}^2}{2n_{p,q,l}^2}+\sigma\left(\Delta x\right)^2(1+\tau), \tag{6b}$$

$$\delta_3=1, \tag{6c}$$

$$\delta_4=\frac{n_{p,q,l}^2+n_{p+1,q,l}^2}{2n_{p,q,l}^2}+\frac{\sigma\left(\Delta x\right)^2\tau}{2}, \tag{6d}$$

$$\sigma=\frac{k_0^2\left(n_{p,q,l}^2-n_{p+1,q,l}^2\right)}{8}, \tag{6e}$$

$$\tau=\frac{3n_{p,q,l}^2+n_{p+1,q,l}^2}{6n_{p,q,l}^2}. \tag{6f}$$

It is noted that the grid points on the edge of the computational window should be dealt with carefully. In order to avoid the nonphysical reflection, the transparent boundary condition (TBC)[21] is applied to approximating these edge points. Moreover, if the field propagates along the imaginary axis (imaginary-distance BPM),[22] the corresponding procedure is efficient to solve the guided-modes for optical waveguides. To treat the S-bent waveguide, we transform the index profile $n(x,\ y)$ into the equivalent straight one $n_{\mathrm{c}}(x,\ y)$ by using the conformal mapping method[18]

$$n_{\mathrm{c}}(x,y)=n(x,y)\left(1+\frac{y}{R}\right), \tag{7}$$

where R is the radius of curvature.

3. Operating principle

The operating principle of the MMI demultiplexer is based on the self-imaging effect, in which the guided-modes of a multimode waveguide are excited and interfere constructively to produce single or

multiple images of an input field launched by a usually single-mode optical waveguide at the one end of the structure at periodic intervals along the direction of propagation.[9−12] Under the restricted interference mechanism, a direct or mirrored image of the injected field is formed at a coupler length of $L_{\mathrm{M}} = pL_{\pi}$ if p is an even or odd integer, respectively, in which L_{π} is the so-called beat length and defined as[12]

$$L_{\pi} = \frac{\pi}{\beta_0 - \beta_1} \approx \frac{4n_g W_{\mathrm{e}}^2}{3\lambda}, \tag{8}$$

where β_0 and β_1 are the propagation constants of the fundamental mode and the first-order mode, respectively. n_{g} is the effective refractive index, W_{e} is the effective width of the fundamental mode of the multimode section, and λ is the light wavelength in free space. To realize the restricted self-imaging effect, the input/out waveguide of a 2×2 MMI coupler should be placed at a lateral offset of $\pm\dfrac{W_{\mathrm{e}}}{6}$, with respect to the centre of the MMI region, so that every third mode will not be excited. As a result, the beat length is three times shorter than that of the general interference mechanism.[12] Moreover, the length of wavelength demultiplexer can be further reduced if a tapered MMI coupler is used.[13] A reduction in length is achieved in the tapered device by reducing the average MMI region width over the length of the structure.

The proposed wavelength demultiplexer is schematically shown in Fig.2. The device consists of three parts: a straight input waveguide, a MMI coupler, and two S-bend output waveguides, in which one is a bar-coupler and the other is a cross-coupler. To make the length of device as short as possible, the tapered MMI coupler under the restricted interference mechanism is introduced into the present demultiplexer as shown in Fig.2.

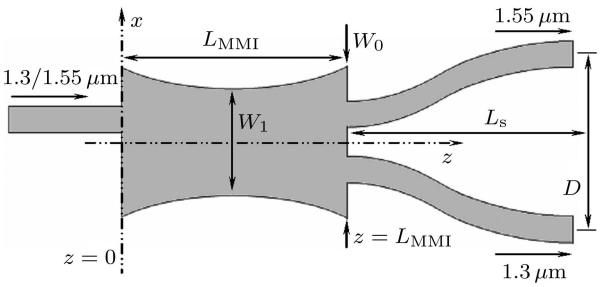


Fig.2. Schematic diagram of a compact wavelength demultiplexer based on the parabolically tapered MMI coupler.

The width of the MMI coupler is parabolically tapered according to the equation given by

$$W(z) = W_1 + (W_0 - W_1)\left(L_{\mathrm{MMI}}/2 - z\right)^2 \Big/ \left(L_{\mathrm{MMI}}/2\right)^2, \tag{9}$$

where W_0 is the width of interference region at $z = L_{\mathrm{MMI}}$ (or z=0) and W_1 is the minimum width at $z = L_{\mathrm{MMI}}/2$. When two waves with wavelengths of $\lambda_1 = 1.30\,\mu$m and $\lambda_2 = 1.55\,\mu$m are injected into the input waveguide, they can be separated from each other if the length L_{MMI} of the tapered MMI coupler satisfies the following relation:

$$L_{\mathrm{MMI}} = pL_{\pi}^{\lambda_1} = (p+q)L_{\pi}^{\lambda_2}, \tag{10}$$

where p is a positive integer, q is an odd integer, and L_{π}^{λ} is the beat length at wavelength λ. As a result, a direct image of the injected field is formed for one wavelength, which corresponds to the bar-state, and a mirrored image is formed for another wavelength, which corresponds to the cross-state. In addition, it has been reported that tilted-waveguides, matched with the local taper angle at the ends of the MMI section, minimize the phase changes due to the discontinuous change in wave fronts present in a taper, but the choice of the angle of the waveguide is a trade-off between the associated power losses and the ease of fabrication and tolerance.[23] In the present study, the straight input waveguide has been considered in the following analysis.

4. Numerical results and discussion

The deep-etched rib waveguide based on the SiO_2/SiON, whose cross section is shown in Fig.3, is utilized in the proposed wavelength demultiplexer. The thicknesses of the upper cladding, the core, and the low cladding are $h_1 = 0.4\,\mu$m, $h_2 = 0.8\,\mu$m, and $h_3 = 0.2\,\mu$m respectively. By using the imaginary-distance procedure with the transverse mesh size of $\Delta x = \Delta y = 0.05\,\mu$m and the propagation step size of $\Delta z = 0.1\,\mu$m, it is found that the rib waveguide with a width of $w = 2.0\,\mu$m only supports the fundamental mode for both λ=1.30 μm and $\lambda = 1.55\,\mu$m. So, the rib width is fixed at $w = 2.0\,\mu$m for both input and output waveguides.

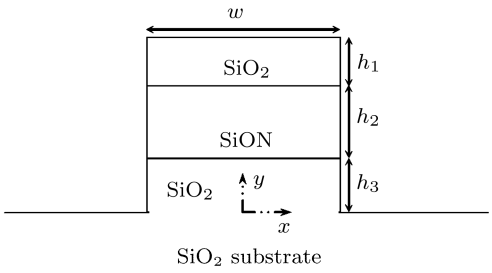


Fig.3. Cross section of a deep-etched rib waveguide.

The field patterns of the fundamental mode in quasi-TE mode (H_y) and in quasi-TM mode (H_x) at wavelength $\lambda = 1.3\,\mu$m are illustrated in Fig.4. It is seen that the mode profiles for H_y and H_x are strongly confined along the x-direction, which ensures that a sufficient number of guided modes supported in the MMI region can image the input field accurately. Therefore, the deep-etched rib waveguide can help to improve the image quality as pointed out in Ref.[9]. In addition, the calculated effective indices of the fundamental mode in quasi-TE and quasi-TM modes are 1.4802 and 1.4799, respectively. The results for the same structure from the mapped Galerkin method[24] and the film mode matching method (FMMM)[25] are 1.4795 and 1.4790, and 1.4800 and 1.4798, respectively. The present results are very close to the solutions from the FMMM, which is so far regarded as a benchmark results for comparing the accuracy.

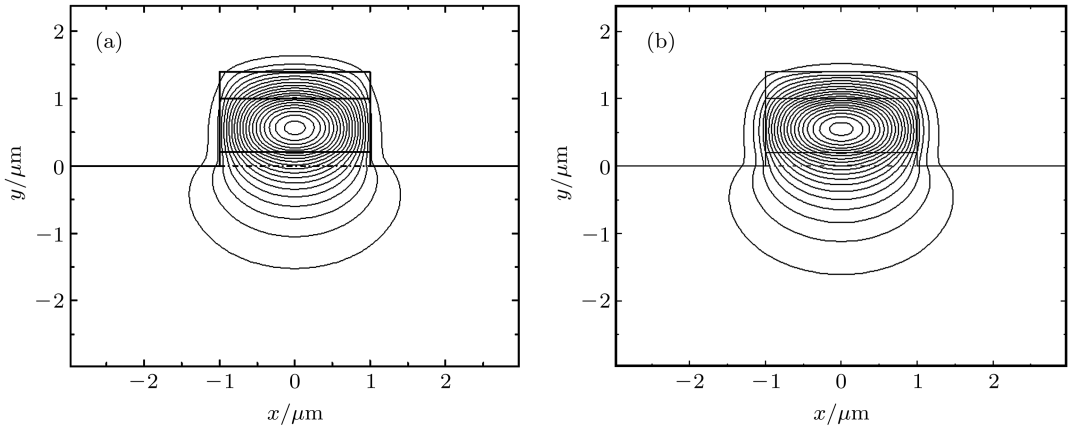


Fig.4. Field patterns of the fundamental mode for a deep-etched rib waveguide: (a) H_y for quasi-TE mode and (b) H_x for quasi-TM mode.

Next, we use the proposed 3D-SV-FD-BPM to calculate the beat lengths and their ratio of the parabolically tapered MMI coupler at $\lambda_1 = 1.30\,\mu$m and $\lambda_2 = 1.55\,\mu$m. Figure 5(a) shows that the beat length as a function of $1 - W_1/W_0$. It is noted that the beat lengths for both wavelengths linearly decrease with the increase of $1 - W_1/W_0$, but increase with the increase of W_0. As a result, tapered MMI coupler can reduce its length. Figure 5(b) shows the ratio $\chi = L_\pi^{\lambda_1}/L_\pi^{\lambda_2}$ as a function of $1 - W_1/W_0$.

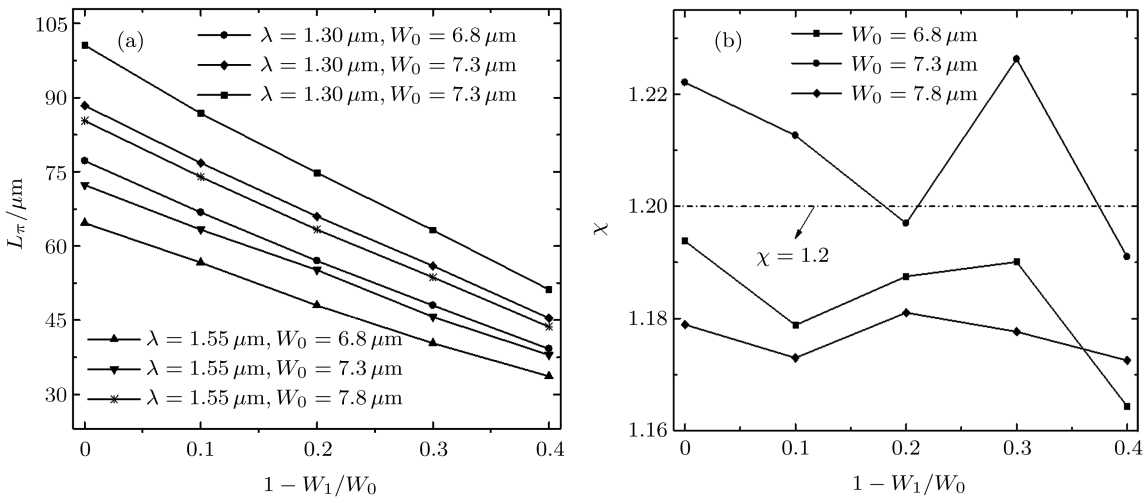


Fig.5. Beat length (a) and their ratio (b) as functions of $1 - W_1/W_0$.

When selecting $W_0 = 7.3\,\mu$m and $1-W_1/W_0 = 0.2$, we obtain a beat length ratio of $1.196 \approx 1.20$, in which the beat lengths for $\lambda_1 = 1.30\,\mu$m and $\lambda_2 = 1.55\,\mu$m are $66.00\,\mu$m and $55.17\,\mu$m, respectively, from Fig.5(a). If $p = 5$ and $q = 1$ in Eq.(10) are selected, the following relation is achieved:

$$330.0\,\mu m = 5L_\pi^{\lambda_1} \approx 6L_\pi^{\lambda_2} = 331.0\,\mu m. \tag{11}$$

Therefore, the tapered MMI region acts as a cross-coupler and bar-coupler at 1.30 and $1.55\,\mu$m wavelengths, respectively. So the two wavelengths can be separated from each other. By using the local guided-mode analysis in Ref.[7], the length of straight MMI coupler with a width of $7.3\,\mu$m is $435.5\,\mu$m. The length of the present tapered MMI coupler is only 76% length of the straight counterpart. However, the beat length ratio of the straight MMI coupler is $\chi = 1.222$ by using the proposed 3D-SV-FD-BPM as show in Fig.5(b).

The performance of the proposed wavelength demultiplexer is assessed by the contrast and insertion loss defined as

$$C = 10\log_{10}\left(\frac{P_1}{P_2}\right), \tag{12a}$$

$$L = -10\log_{10}\left(\frac{P_1}{P_i}\right), \tag{12b}$$

where P_1 and P_2 are the intensities in the bar and cross output waveguides at $\lambda_1 = 1.30\,\mu$m, respectively, or the intensities in the cross and bar output waveguides at $\lambda_2 = 1.55\,\mu$m, respectively, and P_i are the intensity in the input waveguides. The gap width between the two S-bend output waveguides at the end of the device is chosen as $D = 20\,\mu$m with a bent length of $L_\mathrm{s} = 100\,\mu$m so that the bending-loss and the cross-coupling effect between the two output waveguides are negligible from the numerical results by using the present 3D-SV-FD-BPM combined with the conformal mapping method. The fundamental mode of the input waveguide is injected, and the transverse mesh size and propagation step size are $\Delta x = \Delta y = 0.05\,\mu$m and $\Delta z = 0.05\,\mu$m, respectively.

The insertion loss and the contrast as functions of width W_0 $(1 - W_1/W_0 = 0.2)$ are shown in Fig.6(a) and Fig.6(b), respectively. It is seen that the demultiplexer is very sensitive to the structure parameter W_0; especially at $\lambda = 1.30\,\mu$m. The insertion loss and the contrast in quasi-TE mode are greater than those in quasi-TM mode at both wavelengths, but the behaviours are almost similar. Figures 6(c) and 6(d) give the insertion loss and the contrast as functions of length of the tapered MMI coupler L_MMI.

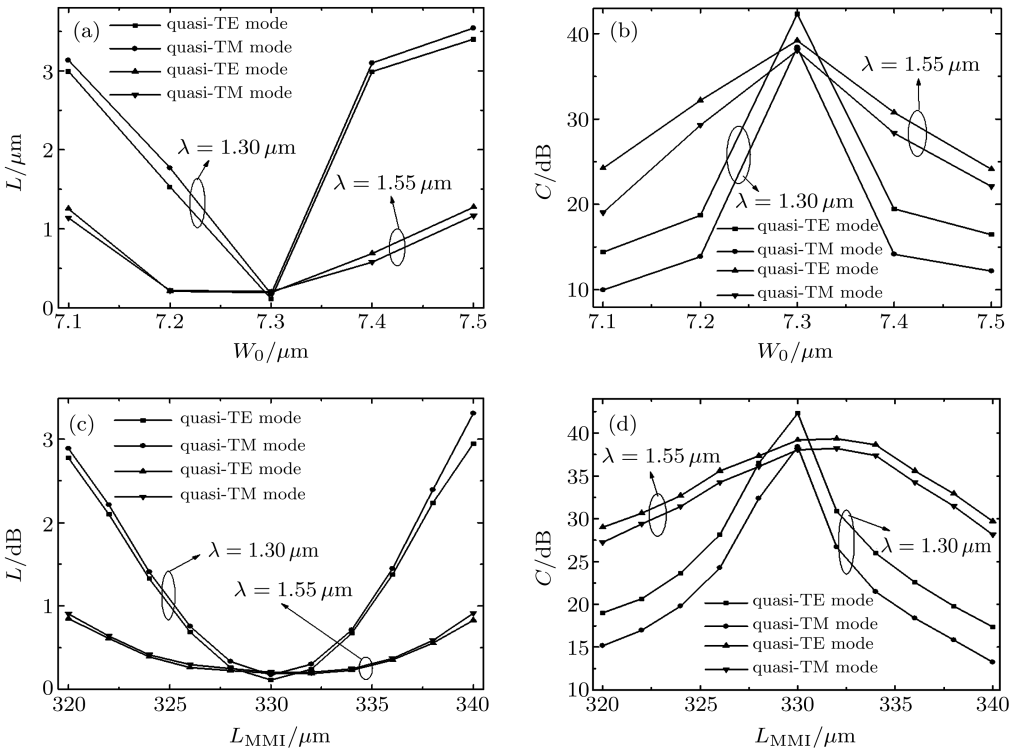


Fig.6. Insertion loss ((a) and (c)) and contrast ((b) and (d)) of the demultiplexer as functions of width W_0 ((a) and (b)) and length L_MMI ((c) and (d)).

Compared with the structure parameter W_0, the demultiplexer is less sensitive to the structure parameter L_{MMI}. For $W_0 = 7.3\,\mu$m and $L_{\mathrm{MMI}} = 330.0\,\mu$m, the insertion losses in quasi-TE mode at $\lambda = 1.30\,\mu$m and $\lambda = 1.55\,\mu$m are 0.11 and 0.19dB, respectively, and the contrasts are 42.3 and 39.2dB, respectively. The same results in quasi-TM mode are 0.17, 0.20, 38.4, and 37.8dB, respectively. So the demultiplexer has a low loss performance. The contrast at $\lambda = 1.30\,\mu$m is greater than at $\lambda = 1.55\,\mu$m, but more sensitive to the structure parameters W_0 and L_{MMI} as shown in Fig.(6).

We also analyse the spectral characteristics of the present demultiplexer. Figure 7 shows the normalized output powers for bar and cross states in quasi-TE mode as a function of the working wavelength from 1.25 to 1.65 μm, in which $W_0 = 7.3\,\mu$m, $1 - W_1/W_0 = 0.2$, and $L_{\mathrm{MMI}} = 330.0\,\mu$m. It is seen that in 1.3 μm window the spectral response is sharp, whilst in 1.55 μm window the spectral response is relatively flat. Moreover, far from the centre wavelengths 1.3 and 1.55 μm, neither bar nor cross state with a high contrast can be obtained. The evolution of the input field along the propagation distance in quasi-TE mode with $y = 0.6\,\mu$m is illustrated in Fig.8. It is noted that the cross-state at $\lambda = 1.30\,\mu$m and bar-state at $\lambda = 1.55\,\mu$m are realized.

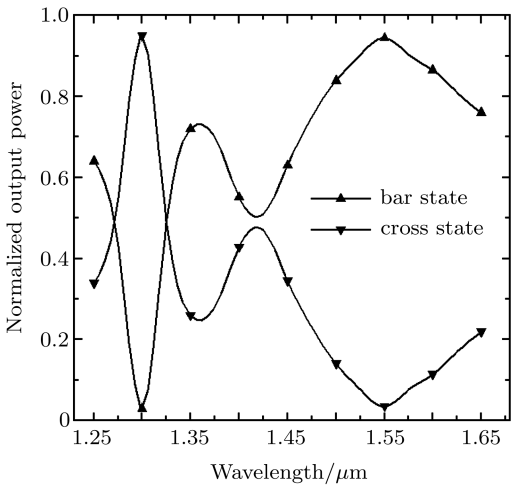


Fig.7. Normalized output power for bar and cross states as a function of wavelength.

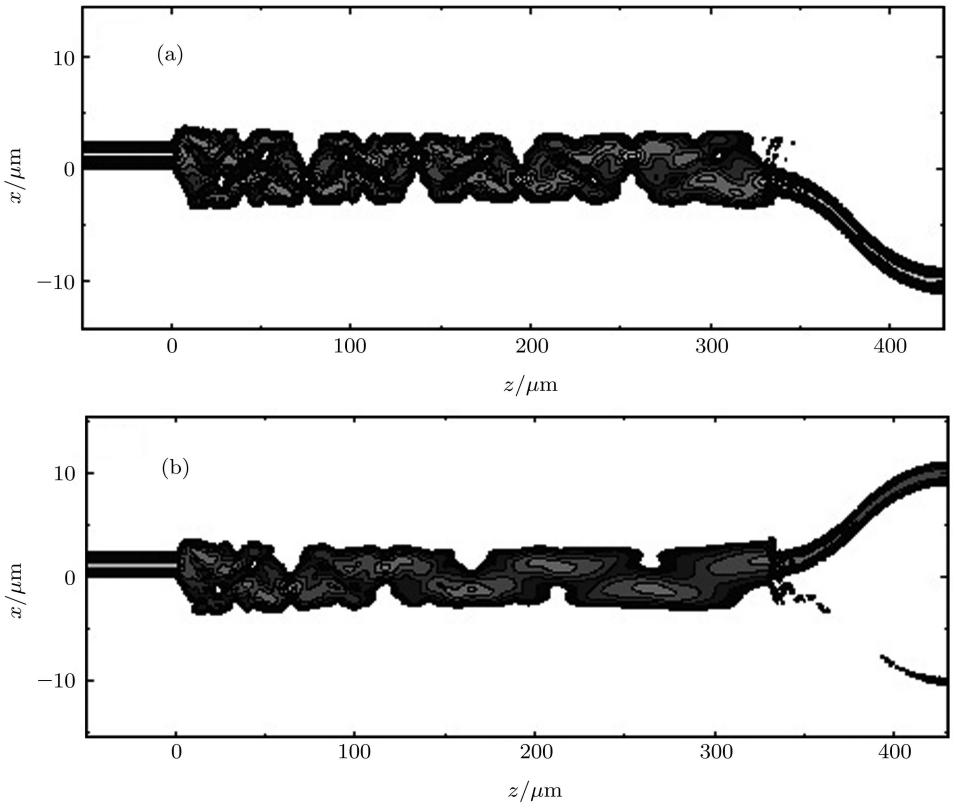


Fig.8. Field distributions in the proposed wavelength demultiplexer with $W_0 = 7.3\,\mu$m, $1 - W_1/W_0 = 0.2$, $L_{\mathrm{MMI}} = 330\,\mu$m, and (a) $\lambda = 1.30\,\mu$m and (b) $\lambda = 1.55\,\mu$m.

5. Conclusions

By using the 3D-SV-FD-BPM based on H field, a compact wavelength demultiplexer based on the parabolically MMI coupler operating at 1.30 and 1.55 μm wavelengths is designed. A short MMI section of 330.0 μm in length, which is only 76% length of the straight MMI coupler, is achieved with the contrasts of 42.3 and 39.2dB in quasi-TE mode, and 38.4 and 37.8 dB in quasi-TM mode at wavelengths 1.30 and 1.55 μm, respectively, and the insertion losses below 0.2 dB at both wavelengths and in both polarization states. Although only the demultiplexing configuration is considered in this paper, the proposed device can also operate as a multiplexer, with the direction of lightwave propagation reversed.

The 3D-SV-FD-BPM is numerically unconditionally stable and is of second-order accuracy in the z-direction since the standard ADI algorithm with the CN scheme is introduced to discretize the resulting equations along the longitudinal direction. Moreover, a modified FD scheme is also constructed to approximate the resulting equations along the transverse directions, in which the discontinuities of the derivatives of magnetic field components H_y and H_x at vertical and horizontal interfaces, respectively, are involved. The light wave propagation in the tapered MMI coupler is demonstrated and the interaction between the output S-bent waveguides is evaluated by using the proposed 3D-SV-FD-BPM combined with the conformal mapping method. In addition, the guided-modes of the deep-etched rib waveguides are solved by using the corresponding imaginary-distance procedure.

References

[1] Shimada T, Sakurai N and Kumozaki K 2005 *J. Lightwave Technol.* **23** 2621

[2] Qin X Y, Huang B Q, Chen H X, Li G and Gu P F 2004 *Acta Phys. Sin.* **53** 3794 (in Chinese)

[3] Hattori K, Kitagawa T, Oguma M, Ohmori Y and Horiguchi M 1994 *Electron. Lett.* **30** 856

[4] Zhang G, Honkanen S, Tervonen A, Wu C M and Najafi I 1994 *Appl. Opt.* **33** 3371

[5] Kolesik M, Matus M and Moloney J V 2003 *IEEE Photon. Technol. Lett.* **15** 78

[6] Paiam M R, Janz C F, Mac Donald R I and Broughton J N 1995 *IEEE Photon. Technol. Lett.* **7** 1180

[7] Lin K C and Lee W Y 1996 *Electron. Lett.* **32** 1259

[8] Li B, Li G, Liu E, Jiang Z, Qin J and Wang X 1999 *IEEE Photon. Technol. Lett.* **11** 575

[9] Soldano L B and Pennings C M 1995 *J. Lightwave Technol.* **13** 615

[10] Xiao J B, Sun X H, Cai C, Zhang X F, Zhu J B and Zhang M D 2003 *Acta Electron. Sin.* **31** 1201 (in Chinese)

[11] Bachmann M, Besse P A and Melchior H 1994 *Appl. Opt.* **33** 3905

[12] Bachmann M, Besse P A and Melchior H 1995 *Appl. Opt.* **34** 6898

[13] Levy D S, Park K H, Scarmozzino R, Osgood R M, Dries C, Studenkov P and Forrest S 1999 *IEEE Photon. Technol. Lett.* **11** 1009

[14] Scarmozzino R, Gopinath A, Pregla R and Helfert S 2000 *IEEE J. Sel. Top. Quantum Electron.* **6** 150

[15] Xiao J B, Sun X H and Zhang M D 2004 *Sci. China Ser.* F **47** 34

[16] Xiao J B and Sun X H 2006 *Chin. Phys.* **15** 1824

[17] Liu P L and Li B J 1992 *IEEE J. Quantum Electron.* **28** 778

[18] Heiblum M and Harris J H 1975 *IEEE J. Quantum Electron.* **QE-11** 75

[19] Press W H, Teukolsky S A, Vetterling W T and Flannery B P 1992 *Numerical Recipes in C-The Art of Scientific Computing* 2nd ed (New York: Cambridge University Press) p827

[20] Yamauchi J, Takahashi G and Nakano H 1998 *IEEE Photon. Technol. Lett.* **10** 1127

[21] Hadley G R 1992 *IEEE J. Quantum Electron.* **28** 363

[22] Chamorro-Posada P 2003 *J. Lightwave Technol.* **21** 862

[23] Themistos C and Rahman B M A 2002 *Appl. Opt.* **41** 7037

[24] Xiao J B, Zhang M D and Sun X H 2004 *J. Opt. Soc. Am.* B **21** 798

[25] Vassallo C 1997 *Opt. Quantum Electron.* **29** 95